**Rare Metal Materials and Engineering**
Volume 51, Issue 8, August 2022
Available online at www.rmme.ac.cn

Science Press

**Cite this article as**: Wang Xinchao, Wang Yan, Hou Lifeng, et al. Corrosion Behavior of Long-Term Aged N10276 Alloy in $CO_2/H_2S/Cl^-$ Environments[J]. Rare Metal Materials and Engineering, 2022, 51(08): 2754-2760.

ARTICLE

# Corrosion Behavior of Long-Term Aged N10276 Alloy in $CO_2/H_2S/Cl^-$ Environments

**Wang Xinchao[1,2], Wang Yan[2], Hou Lifeng[1], Zhang Shaohua[3], Liu Baosheng[3], Wei Yinghui[1]**

*[1] College of Materials Science and Engineering, Taiyuan University of Technology, Taiyuan 030024, China; [2] State Key Laboratory of Advanced Stainless Steel Materials, Taiyuan Iron & Steel (Group) Co., Ltd, Taiyuan 030003, China; [3] College of Materials Science and Engineering, Taiyuan University of Science and Technology, Taiyuan 030024, China*

**Abstract:** The corrosion mechanism of the N10276 alloy before and after long-term aging treatment in aqueous solutions containing $CO_2/Cl^-$ and $CO_2/H_2S/Cl^-$ was studied through the electrochemical impedance plots and cyclic potentiodynamic polarization. Results reveal that a not-well-defined capacitive loop appears in the low-frequency range and it changes into Warburg's impedance as the $H_2S$ concentration increases (10~100 μL/L) due to the large quantities of $H_2S$-related adsorbed species in the film. In addition, $H_2S$ concentration plays a key role in increasing corrosion rate. In comparison, the action of long-term aging is more significant on pitting corrosion. The surrounding sites of the precipitates become the preferred corrosion area since the austenite microstructure of long-term aged N10276 alloy includes lots of precipitated second phases ($\mu$ phase with accumulation of Mo and Ni elements), leading to the occurrence of pitting defects.

**Key words:** corrosion mechanism; N10276 alloy; long-term aging; $H_2S$

Recently, the increasing demand of energy has attracted tremendous interest in extraction of deep sour fields ($H_2S$ containing) in oil and gas wells[1,2]. $CO_2$ and $H_2S$ are prevalent in the production stream of natural $CO_2/H_2S$ gas production, accompanied with $H_2O$ from reservoirs[3]. Meanwhile, $H_2S$ can partially dissolves in the aqueous phase to form a chemical equilibrium system ($H_2S/HS^-/S^{2-}/H^+$) by a series of complex depolarization processes[4], contributing to the elevation of solution acidity. When the inner surface of conventional pipelines contacts with highly corrosive liquid flow ($CO_2/H_2S/H_2O$) in the extraction, refining and transport processes of oil and gas, the pipelines will suffer irreversible corrosion damage and even brittle failure[5]. Thus, employing Ni-based corrosion resistant alloy is significantly vital for improving mechanical performance and reducing equipment failure risk.

Several studies have been carried out on the corrosion behavior of low carbon steel or conventional stainless steels in environments containing $CO_2/H_2S/Cl^-$ by mathematical models[6], corrosion kinetics[7], innovative electrochemical techniques[8], etc, which enhance the understanding of the corrosion mechanism of conventional metallic materials. N10276 alloy is one of the main materials serving the "sour" oil and gas industries, such as tubes and a variety of other underground and ground components. With a high nickel and chromium content, N10276 alloy is superior to carbon and alloy steel in corrosion resistance[9,10], which can form more protective passive film in harsh environment. In addition, the N10276 is alloyed by approximately 15wt% ~17wt% molybdenum (Mo). As a result, the alloy exhibits excellent resistance to pitting corrosion in the $Cl^-$-containing environment and good weldability[11]. However, sensitization is still one of the main problems during welding or heat treatments, though the low carbon content of the N10276 alloy minimizes carbide precipitation to maintain resistance to intergranular attack[12]. Many studies have proven that chromium carbide forms at grain boundaries and the appearance of chromium carbide ($Cr_{23}C_6$) compounds results in the formation of chromium-depleted zones[13,14]. It is

Received date: August 13, 2021
Foundation item: National Natural Science Foundation of China (52071227); Special Found Projects for Central Government Guidance to Local Science and Technology Development (YDZX20181400002967); Key Scientific Research Project in Shanxi Province (201805D121003, 201903D111008, 201901D111460, 202003D111001); Science and Technology Major Projects of Shanxi Province (20191102004, 20201102017)
Corresponding author: Wei Yinghui, Ph. D., Professor, College of Materials Science and Engineering, Taiyuan University of Technology, Taiyuan 030024, P. R. China, Tel: 0086-351-6018683, E-mail: yhwei_tyut@126.com

noteworthy that the saturation of carbon in austenite is less than 0.02%, and thus the chromium-depleted zones are obviously not applicable in the N10276 alloy since its carbon content is generally lower than 0.02%. In comparison, the precipitates will inevitably appear with the extension of service time when this alloy is used in a long-term high-temperature environment, which seriously destroys the corrosion resistance of the material. Therefore, the effect of long-term aging on the properties of corrosion-resistant alloys cannot be ignored. Up to now, the research on the N10276 alloy mainly focuses on the hot working properties, medium temperature brittleness and welding properties[15-17]. In addition, there are few studies on the corrosion behavior of the N10276 alloy after long-term aging under the conditions of dissolved $CO_2$, $H_2S$ and $Cl^-$. This is a challenging condition since severe pitting, or even the threat of unexpected material failure may happen due to the activation of potential difference with increasing $H_2S$ concentration. Therefore, it is highly desirable to study the effect of long-term aging on the corrosion behavior of N10276 alloy in an environment containing dissolved $CO_2$, $H_2S$ and $Cl^-$.

In the current research, an attempt was made to present new results for the corrosion behavior of the N10276 alloy before and after long-term aging in aqueous solutions containing $CO_2$/$Cl^-$ and $CO_2$/$H_2S$/$Cl^-$ at various concentrations of $H_2S$ (10~100 μL/L). The microstructure and electrochemical property of the N10276 alloy were studied by characterization, electrochemical impedance spectroscopy (EIS) and cyclic potentiodynamic polarization tests. Finally, the corresponding corrosion mechanism was clarified.

## 1 Experiment

### 1.1 Materials and sample preparation

Cold rolled sheet of N10276 alloy was used, and its chemical composition (wt%) was C 0.007, Si 0.04, Mn 0.52, P 0.008, S 0.002, Cr 15.22, Mo 15.56, W 3.35, Fe 6.24, and the balance Ni. N10276 alloy was solution annealed in a box resistance furnace at 1160 °C for 1 h and quenched in water to ensure the uniformity of the material, which was designated as original alloy. Subsequently, in order to study the effect of long-term aging treatment on corrosion resistance, the N10276 alloy was aged at 800 °C for 1000 h, which was designated as long-term aged alloy. The alloys before and after long-term aging were processed into rectangular samples (20 mm×20 mm×1.7 mm). The preparation process included wet-grinding specimens with SiC grit paper up to 2000 grit, cleaning by deionized water, acetone and high purity ethanol, and drying by compressed air. Samples prepared for microstructure inspection were etched by aqua regia ($HCl:HNO_3$= 3:1, volume ratio). The microstructure formed after long-term aging was characterized by optical metallography, scanning electron microscope (SEM), energy disperse spectrum analyzer (EDS) and transmission electron microscope (TEM). The possible phases in N10276 alloy under equilibrium conditions were calculated by Thermo Calc software.

### 1.2 Electrochemical tests

All testing solutions were performed by dissolving analytical grade NaCl (3.5wt% ) in deionized water. Each solution was purged at least 2 h in advance and $CO_2$ was bubbled into the solution to ensure saturation. The required concentrations of $H_2S$ were achieved by the reaction of sulfuric acid with sodium sulfide in the abovementioned stock solution at 0, 10 and 100 μL/L, based on the stoichiometry[18]:

$$H_2SO_4 + Na_2S \rightarrow Na_2SO_4 + H_2S \quad (1)$$

The measurements were carried out in the conventional three-electrode cell consisting of a saturated calomel electrode (SCE) as the reference electrode (RE), a platinum plate as the counter electrode (CE) and a working electrode (WE). The working electrode was mounted in a self-cured epoxy resin to offer an exposed surface area of 1 $cm^2$. The scanning rate was 1 mV/s, and the potential scanning ranged from −0.2 V to 1.0 V vs. SCE in forward scans and then was reversed to −0.2 V vs. SCE. Then, the EIS measurements were carried out on the OCP with a linear perturbation (amplitude: often 10 mV peak-to-peak) in a frequency range of $10^5$ Hz to $10^{-2}$ Hz. In all of the experiments, the solution in the electrochemical autoclave was efficiently stirred by a magnetic agitator at 60 r/min. All electrochemical measurements were conducted at 30 °C for at least five times, in which the representative curve of each condition was selected for analyzing the electrochemical reactions. To elucidate the corrosion behavior of the N10276 alloy, the specimens after the electrochemical measurements were further characterized by scanning electron microscope (SEM, Hitachi S-4800) coupled with energy disperse spectroscopy (EDS, OXFORD).

## 2 Results and Discussion

### 2.1 Characterization of microstructure before and after long-term aging

As shown in Fig. 1, the microstructures of the original and long-term aged N10276 alloy samples are typical austenitic structure, and the precipitates are completely dissolved in the matrix (Fig. 1a). After long-term aging treatment, the sample surface becomes rougher. A large number of precipitates can be observed at the boundaries and accompanied by annealing twin boundaries and grains (Fig.1b).

The thermodynamic equilibrium phase diagram of N10276 alloy was calculated by thermodynamic calculation software Thermol-Calc. As can be seen from Fig. 2, single-phase austenite structure is obtained preferentially after the solidification of N10276 alloy. When the temperature is below 1110 °C, $M_6C$ phase precipitates in austenite matrix. With decreasing the temperature below 1030 °C, $\mu$ phase increasingly precipitates from the austenite. At 800 °C, the mass fraction of $\mu$ phase (14.13wt%) is much higher than that of $M_6C$ carbide (0.29wt%). Therefore, the $\mu$ phase is considered to be the main precipitate affecting the properties of N10276 alloy.

According to the energy dispersive spectrum (EDS) analysis of precipitates after long-term aging, the components

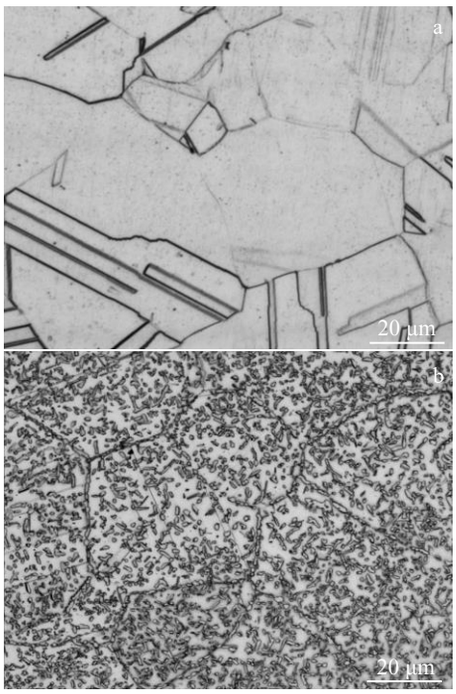


Fig.1 Microstructures of N10276 alloy before (a) and after (b) long-term aging treatment

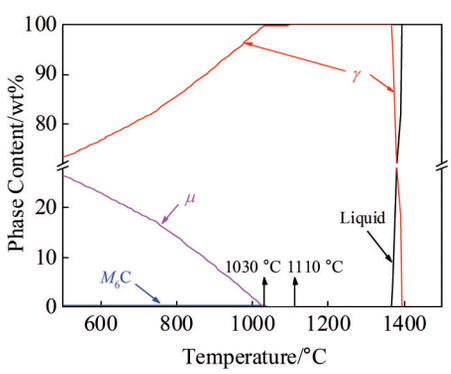


Fig.2 Thermodynamic phase diagram of N10276 alloy

of precipitates at different positions are very similar, i. e., mainly Mo and Ni elements, as well as W and Cr elements. Moreover, the TEM image and selected area electron diffraction (SAED) patterns of long-term aged N10276 alloy are shown in Fig.3. It confirms that the precipitated phases are $\mu$ phase and $M_6C$ carbide. The $\mu$ phase is distributed along grain boundaries, while a small amount of $M_6C$ carbides only appear at partial grain boundaries. The $M_6C$ carbide precipitates at the grain boundary can provide nucleation sites for the precipitation of $\mu$ phase[16]. This also proved that $\mu$ phase is the main precipitate of N10276 alloy after long-term aging.

### 2.2 Electrochemical impedance spectroscopy

Electrochemical impedance spectroscopy tests were conducted to understand the corrosion process of the original and long-term aged N10276 alloy in the $CO_2$-saturated 3.5wt% NaCl solutions containing various $H_2S$ contents. The Nyquist, Bode magnitude and Bode phase plots of the resulted EIS data are shown in Fig. 4. Firstly, the Nyquist plots obtained from the specimens in the saturated $CO_2$ solution exhibit a high-frequency (*f*) capacitive loop which is always associated with the double layer relaxation[19]. In addition, the tests of specimens in the $CO_2$-saturated NaCl solutions containing 10~100 μL/L dissolved $H_2S$ indicate that the interfacial reactions at the high-frequency range are very similar to that of the former. The reduction of impedance radius that corresponds to the obvious increase of corrosion rate can be explained by the accelerated cathodic hydrogen evolution reactions as a result of the decrease of pH values with the injection of dissolved $H_2S$[8]. In comparison, an important observation is the obvious changes of impedance plots at the low-frequency range with the elevation of $H_2S$ content. For instance, for the 10 μL/L $H_2S$ case, another not well-defined capacitive loop appears at the low-frequency range, whilst it changes into a straight line (Warburg's impedance) with increasing the $H_2S$ concentration to 100 μL/L. The appearance of Warburg's impedance suggests that the corrosion of the specimens in the $CO_2$-saturated NaCl solutions containing 100 μL/L $H_2S$ may originate from the mass transport to some extent[19,20]. Absorbed layer involving high quantities of $H_2S$-related species or even corrosion products will form on the specimen surfaces when the N10276 alloy specimens are immersed in the solution, and the

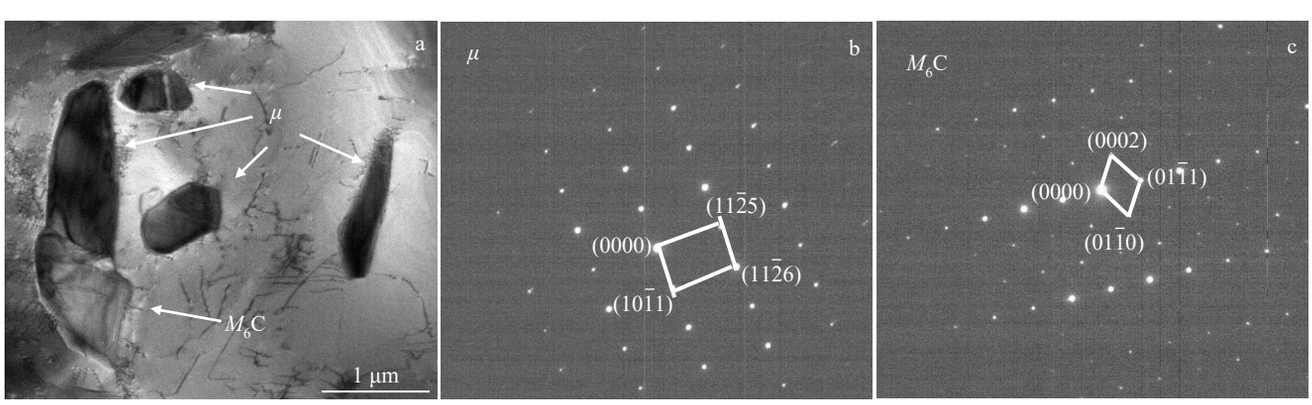


Fig.3 TEM image (a) and SAED patterns (b, c) of precipitates in N10276 alloy

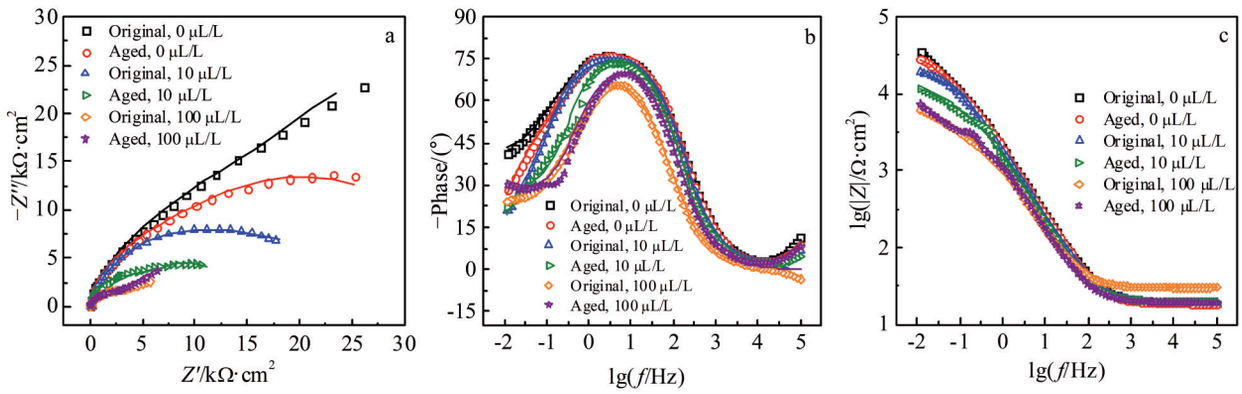


Fig.4 Electrochemical impedance spectroscopy of the original and long-term aged N10276 alloy exposed to the $CO_2$-saturated 3.5wt% NaCl solutions containing various $H_2S$ contents involving Nyquist curve (a), Bode phase (b) and Bode plots (c) at 30 °C

absorbed species on the steel surfaces also behave as films, through which the transfer process of corrosion reactants and the diffusion of soluble species are proceeded[21]. In addition, the long-term aged N10276 alloy with various $H_2S$ concentrations results in decrease of high-frequency capacitive loop radius, which is mainly associated with heterogeneous element distribution and unstable passive films after the long-term aging treatment.

In order to explain the interfacial reaction kinetics of the original and long-term aged N10276 alloy samples in $CO_2$-saturated NaCl solution of various $H_2S$ concen-trations, an equivalent circuits analysis was performed by the equivalent circuits to fit the impedance plots, e.g., $R(QR)$, $R(Q(R(QR)))$ and $R(Q(RW))$ corresponds to $H_2S$ concentrations at 0, 10 and 100 μL/L, respectively. As shown in Fig. 5 and Table 1, and the circuits are suitable for the experimental data in the corresponding systems. The elements in the equivalent circuits analysis are: solution resistance ($R_s$); double-layer capacitance between the metallic substrate and electrolyte, which can be represented as $CPE_{dl}$, the constant phase element exponent (phase shift, $n_{dl}$), and the charge transfer resistance ($R_{ct}$). A parallel combination of film capacitance ($CPE_f$), the constant phase element exponent (phase shift, $n_f$), and the corresponding film resistance ($R_f$) appear in the circuit. In addition, $W$ is Warburg's impedance. The constant phase element (CPE) is introduced in the equivalent circuit instead of pure double layer capacitance. The aim is to reduce the

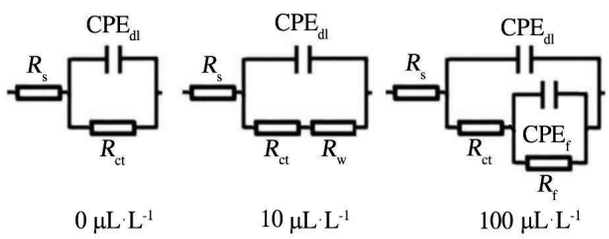


Fig.5 Corresponding equivalent circuit diagrams of resulted EIS data of the original and long-term aged N10276 alloy specimens exposed to the $CO_2$-saturated 3.5wt% NaCl solutions containing different $H_2S$ contents

effect of surface irregularities and compositional inhomogeneity of the steels[22]. The impedance of CPE is defined in Eq.(2).

$$Z_{CPE} = \frac{1}{Y_0}(j\omega)^{-n} \quad (2)$$

where $Y_0$ is the magnitude of CPE, $\omega = 2\pi f$ is the angular frequency, $f$ is the ordinary frequency (measured in Hz), j is the imaginary number and $n$ is the dispersion coefficient related to surface non-homogeneity. Depending on the value of $n$, CPE may be pure resistor (i.e., if $n$=0, then $Z_0$=$R$), pure capacitor (meaning that $n$=1 when $Z_0$ = $C$) or inductor (i.e., when $n$=0.5 and $Z_0$ =$W$)[23]. It can be seen from Table 1 that the long-term aged N10276 alloy exhibits a relatively lower $R_{ct}$ values compared to original N10276 alloy, and this effect can

**Table 1 Parameters of electrochemical impedance spectroscopy component of specimens in the $CO_2$-saturated 3.5wt% NaCl solutions containing various $H_2S$ contents**

| Specimen | $H_2S$ concentration/ μL·L$^{-1}$ | $R_s$/ Ω·cm$^2$ | $CPE_{dl}$/ ×10$^{-4}$ F·cm$^{-2}$ | $n_{dl}$ | $R_{ct}$/ Ω·cm$^2$ | $CPE_f$/ ×10$^{-4}$ F·cm$^{-2}$ | $n_f$ | $R_f$/ Ω·cm$^2$ | $W$/ ×10$^{-4}$·cm$^{-2}$ |
|---|---|---|---|---|---|---|---|---|---|
| Original N10276 | 0 | 19.42 | 1.018 | 0.8725 | 38050 | - | - | - | - |
| | 10 | 19.30 | 1.123 | 0.8697 | 17040 | 6.095 | 0.8 | 18600 | - |
| | 100 | 29.91 | 1.845 | 0.8405 | 3211 | - | - | - | 10.08 |
| Long-term aged N10276 | 0 | 18.95 | 1..052 | 0.8712 | 21480 | - | - | - | - |
| | 10 | 20.01 | 1.167 | 0.8908 | 7268 | 9.021 | 0.9237 | 6973 | - |
| | 100 | 19.61 | 1.505 | 0.8771 | 2992 | - | - | - | 8.115 |

be attributed to micro-galvanic effect (the precipitates serve as preferred area of corrosion); however, this trend is insignificant in the case of 100 μL/L $H_2S$, and it might be related to the formation of massive sulfide compounds (like $FeS_2$ and $MoS_2$) as corrosion product films[24]. Besides, the values of $R_{ct}$ for the original and long-term aged N10276 alloy samples considerably decrease with increasing $H_2S$ concentration, indicating faster rate of reactions at the matrix/electrolyte interface[25].

### 2.3 Cyclic potentiodynamic polarization

The cyclic potentiodynamic polarization results for the original and long-term aged N10276 alloy samples in the $CO_2$-saturated 3.5 wt% NaCl solution containing various concentrations of $H_2S$ are shown in Fig. 6. The corrosion current density can be obtained by the Tafel fitting method for anodic and cathodic regions. The corrosion potential ($E_{corr}$), corrosion current density ($i_{corr}$) and pitting potential ($E_{pit}$) were extracted to compare the changes in the corrosion resistance of long-term aged and original N10276 alloy at various concentrations of $H_2S$, as indicated in Table 2 and Fig. 7. Firstly, the $E_{pit}$ values of original samples are more positive than that of long-term aged samples at various $H_2S$ concentrations, indicating that the long-term aging treatment results in the decrease in the resistance to pitting and localized corrosion[26]. On the other hand, the $E_{pit}$ values of the original and long-term aged N10276 alloy samples gradually decrease with increasing $H_2S$ concentration. In addition, similar to the case of describing $E_{pit}$ values, $E_{corr}$ exhibits a relatively lower value under the conditions of the long-term aging treatment and higher $H_2S$ concentration. From another perspective, for original N10276 alloy, the cyclic polarization curve shows a negative hysteresis (reverse scan current density is less than that for the forward scan) accompanied by the elevation of corrosion potential, which is associated with the end in the growth of initiated pits[27]. In comparison, for the long-term aged N10276 alloy specimens at various $H_2S$ concentrations, positive or parallel hysteresis can be observed, and it is always related to the continuous growth of corrosion pits[28]. It can be concluded from the abovementioned results that $H_2S$ concentration plays a key role in increasing corrosion rate, whereas the effect of long-term aging treatment on pitting corrosion is more significant since the positive or parallel hysteresis is obvious after long-term aging treatment.

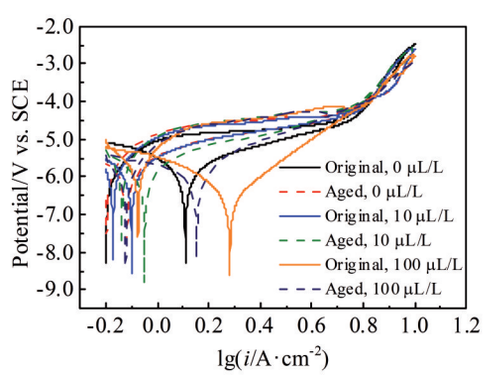


Fig.6 Cyclic potentiodynamic polarization curves of the original and long-term aged N10276 alloy in the $CO_2$-saturated 3.5wt% NaCl solution containing different contents of $H_2S$

**Table 2 Parameters of potentiodynamic polarization curves of the original and long-term aged N10276 alloy in the $CO_2$-saturated 3.5wt% NaCl solutions containing various $H_2S$ contents**

| Specimen | $H_2S$ concentration/μL·L$^{-1}$ | $E_{corr}$/V vs. SCE | $i_{corr}$/μA·cm$^{-2}$ |
|---|---|---|---|
| Original N10276 | 0 | -0.197 | 0.328 |
| | 10 | -0.136 | 0.683 |
| | 100 | 0.072 | 0.890 |
| Long-term aged N10276 | 0 | -0.203 | 0.500 |
| | 10 | -0.175 | 0.802 |
| | 100 | -0.112 | 0.948 |

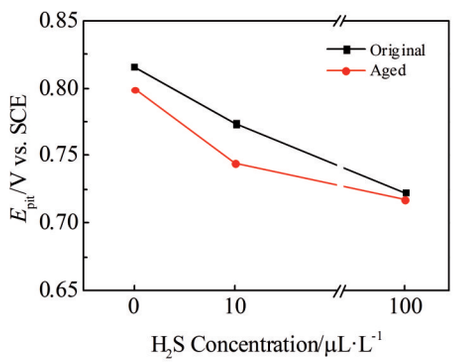


Fig.7 Variation of $E_{pit}$ of the original and long-term aged N10276 alloy in the $CO_2$-saturated 3.5wt% NaCl solutions containing various $H_2S$ contents at 30 °C

### 2.4 Surface profiles of the N10276 alloy specimens after cyclic potentiodynamic polarization measurements

Fig. 8 describes the profiles of specimen surfaces after the cyclic potentiodynamic polarization measurements in the $CO_2$-saturated 3.5wt% NaCl solution containing various concentrations of $H_2S$. In case of the original and long-term aged N10276 alloy specimens, the degree of corrosion is slightly enhanced with increasing $H_2S$ concentration. For the original N10276 alloy, most of the specimen steel surfaces maintain its original features, accompanied by several single corrosion pits with small sizes. In comparison, the surface morphologies of N10276 alloy specimens after long-term aging treatment are characterized with obvious corrosion pits, which is in good agreement with the electrochemical results. Based on the experimental results, the action mechanism of $H_2S$ concentration and long-term aging treatment can be clarified as follows. Firstly, Cr element in N10276 alloy can form dense $Cr_2O_3$ and $Cr(OH)_3$ passive films on the surface of steel, whilst the high valence molybdenum ion (such as $Mo^{6+}$) exists in the film, and some active positions will be quickly

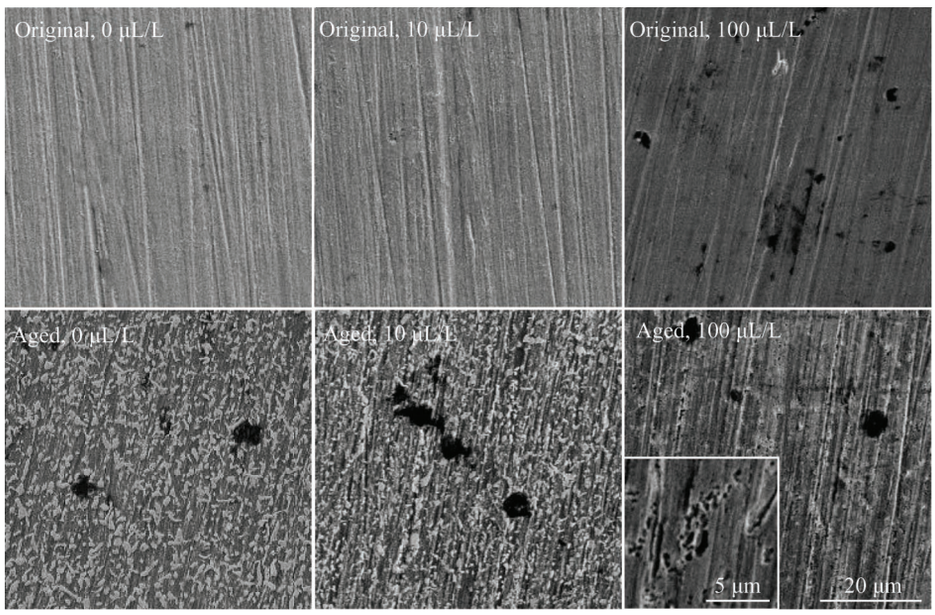


Fig.8 Surface morphologies of original and long-term aged N10276 alloy after the cyclic potentiodynamic polarization measurements in the $CO_2$-saturated 3.5wt% NaCl solution containing various concentrations of $H_2S$

covered by molybdenum hydroxide and molybdate to prevent further corrosion of the matrix, even though the specimens are immersed in some severe environments containing massive corrosive species[29]. In comparison, many molybdenum-depleted sites will be formed to great degree since the austenite microstructure of long-term aged N10276 alloy includes lots of precipitates ($\mu$ phase with accumulation of Mo and Ni elements), leading to the instability of formed passive film at the molybdenum-depleted position, and these sites will become the preferred corrosion area, through which the corrosive species can contact and attack the surface of N10276 alloy. Previous literatures have reported that the thinner film is related to higher electrical field strength and consequently to a larger migration of the dissolved metal ions[30]. As such, the destruction of $Cl^-$ to pitting corrosion has been enhanced under the condition of external anodic polarization. In the meanwhile, the walls of pits are anodic sites with negative potential whereas the passive film is in a passive state with positive potential, and some micro-galvanic corrosion battery forms (large cathode vs. small anode), promoting the gradual expansion of corrosion pits.

## 3 Conclusions

1) Precipitates of N10276 alloy after long-term aging are $\mu$ phase and $M_6C$ carbide. Among them, $\mu$ phase is the main precipitate phase. The two precipitation phases are similar in composition, which are mainly Mo and Ni elements, and contain a large amount of W and Cr elements.

2) The obvious change of impedance plots can be observed, involving another not well-defined capacitive loop in the low-frequency range and it changes into Warburg's impedance in the cases of 10~100 μL/L $H_2S$ concentrations.

3) The enhanced corrosion behavior can be observed under the conditions of the long-term aged treatment and higher $H_2S$ concentration. $H_2S$ concentration plays a key role in increasing the corrosion rate, whereas the effect of long-term aging on pitting corrosion is more significant since the positive or parallel hysteresis is obvious after the long-term aging treatment.

4) The action mechanism of long-term aging treatment can be clarified as follows: the surrounding sites (Cr/Mo-depleted) of the precipitates will become the preferred corrosion area to great degree since the austenite microstructure of long-term aged N10276 alloy includes lots of precipitated second phase ($\mu$ phase and $M_6C$), leading to the occurrence of lots of pitting defects.

## References

1 Liu Z G, Gao X H, Du L X *et al. Materials and Corrosion*[J], 2016, 68(5): 566

2 Wang Xia, Zhou Wenjie, Hou Duo *et al*. *Rare Metal Materials and Engineering*[J], 2020, 49(11): 3734

3 Wen Xiangli, Bai Pengpeng, Luo Bingwei *et al*. *Corrosion Science*[J], 2018, 139:124

4 Chen Changfeng, Jiang Ruijing, Zhang Guoan *et al*. *Rare Metal Materials and Engineering*[J], 2010, 39(3): 427 (in Chinese)

5 Bai Z Q, Yin Z F, Wei D *et al. Materials and Corrosion*[J], 2010, 61(8): 689

6 Banaś J, Lelek-Borkowska U, Mazurkiewicz B *et al. Electrochimica Acta*[J], 2007, 52(18): 5704

7 Zhang Zhi, Zhang Naiyan, Liu Zhiwei *et al. Materials and Corrosion*[J], 2018, 69(3): 386

8 Zhang G A, Zeng Y, Guo X P *et al. Corrosion Science*[J], 2012, 65: 37

9 Zhang Jie, Li Bowen, Li Yanhui *et al. International Journal of Hydrogen Energy*[J], 2021, 46(42): 22 222

10 Qiu Zhijun, Wu Bintao, Zhu Hanliang *et al. Materials & Design* [J], 2020, 195: 109 007

11 Bal K S, Majumdar J D, Choudhury A R. *Corrosion Science*[J], 2019, 175: 406

12 Aydoğdu G H, Aydinol M K. *Corrosion Science*[J], 2006, 48(11): 3565

13 Wang Jiaxu, Shi Wei, Xiang Song *et al. Corrosion Science*[J], 2021, 181: 109 234

14 Vignal V, Zhang H, Delrue O *et al. Corrosion Science*[J], 2011, 53(3): 894

15 Zhang Chi, Zhang Liwen, Shen Wenfei *et al. Journal of Alloys and Compounds*[J], 2017, 728: 1269

16 Pu Enxiang, Zheng Wenjie, Song Zhigang *et al. Materials Science and Engineering A*[J], 2018, 714: 59

17 Ramkumar K D, Joshi V, Pandit S *et al. Materials & Design*[J], 2014, 64: 775

18 Ma Houyi, Cheng Xiaoliang, Li Guiqiu *et al. Corrosion Science* [J], 2000, 42(10): 1669

19 Keddam M, Mottos O R, Takenouti H. *Chemischer Informationsdienst*[J], 1981, 12(23): 257

20 Skale S, Dolecek V, Slemnik M S. *Corrosion Science*[J], 2007, 49(3): 1045

21 Zhang Shaohua, Hou Lifeng, Du Huanyun *et al. Corrosion*[J], 2019, 75(9): 1034

22 Yamina B, Kamel B, Marie T *et al. Materials and Corrosion*[J], 2019, 70(2): 206

23 Luo H, Dong C F, Li X G *et al. Electrochimica Acta*[J], 2012, 64: 211

24 Hesketh J, Dickinson E, Martin M L *et al. Corrosion Science*[J], 2021, 184: 109 265

25 Onyeji L, Mohammed S, Kale G. *Corrosion Science*[J], 2018, 138: 146

26 Li Longyi, Yan Jing, Xiao Jie *et al. Corrosion Science*[J], 2021, 187: 109 472

27 Mills D J. *Progress in Organic Coatings*[J], 1995, 26(1): 73

28 Sun Li, Sun Yangting, Lv Chenxi *et al. Corrosion Science*[J], 2021, 185: 109 432

29 Meguid E A A E, Latif A A A E. *Corrosion Science*[J], 2007, 49(2): 263

30 Kolotyrkin J M. *Journal of the Electrochemical Society*[J], 1961, 108(3): 209


# 长期时效N10276合金在$CO_2/H_2S/Cl^-$环境中的腐蚀行为


王鑫潮[1,2]，王　岩[2]，侯利锋[1]，张少华[3]，刘宝胜[3]，卫英慧[1]

(1. 太原理工大学 材料科学与工程学院，山西 太原 030024)

(2. 太原钢铁(集团)有限公司 先进不锈钢材料国家重点实验室，山西 太原 030003)

(3. 太原科技大学 材料科学与工程学院，山西 太原 030024)



**摘　要：**通过电化学阻抗与循环动电位极化的方法研究了在$CO_2/Cl^-$以及$CO_2/H_2S/Cl^-$溶液体系中、长期时效前后N10276合金的腐蚀机理。结果表明，阻抗弧的低频区间出现了一个不完整的容抗弧，并且随$H_2S$浓度的增加（10~100 μL/L）转变为Warburg阻抗，其主要原因是高含量$H_2S$相关吸附物。$H_2S$可以增加合金腐蚀速率。相比较而言，长期时效处理主要作用于合金点蚀的形成，其中，经过长期时效处理的奥氏体组织内存在大量的第二相（富含Mo与Ni的$\mu$相），而析出物周围的区域成为优先腐蚀区域，进而导致了N10276合金点蚀的发生。



**关键词：**腐蚀机理；N10276合金；长期时效；$H_2S$



作者简介：王鑫潮，男，1989年生，博士生，太原理工大学材料科学与工程学院，山西 太原 030024，E-mail：wangxinchao0017@link.tyut.edu.cn